Electrically Induced Inertial Dynamical Depolarization in Ferroelectric Capacitors for Nanosecond High-Voltage Pulse Generation, with a Calibrated Transmission-Line Reference Source - Focused for Efficient Non-Equilibrium Plasma Formation

M. Ganciu[1,2], P. A. Sebe[1], V. Cionga[1] and A. Ludu[3]

[1] *Ferrodynamics Systems, Bucharest, Romania*
[2] *IT Center for Science and Technology, Bucharest, Romania*
[3] *Embry-Riddle Aeronautical University, Department of Mathematics & Wave Lab, Daytona Beach, FL 32114, USA*

(Received: 25. May 2026, Accepted: 23. July 2026, Published online: 27. July 2026)

Inertial polarization dynamics predicted by the Landau–Khalatnikov–Tani (LKT) model have lacked direct experimental confirmation in bulk ferroelectrics. We report electrically induced inertial dynamical depolarization in pre-polarized $BaTiO_3$ and PZT capacitors at room temperature, producing sub-5-ns high-voltage pulses and underdamped oscillations in the 90–200 MHz range. Above a critical threshold V_C, the polarization trajectory crosses the LKT separatrix, driving the system from a high-permittivity overdamped state into a low-permittivity underdamped regime with rapid release of stored energy. The inertial origin is established by two independent linear controls: a linear polypropylene-film capacitor of identical capacitance reproduces neither the voltage threshold nor the elevated post-transition frequency, and a spark-gap-only transmission-line reference produces no underdamped ringing. The higher post-transition frequency observed exclusively with the ferroelectric capacitor indicates a dynamic collapse of effective permittivity upon separatrix crossing, quantified as $C_{\text{eff}} = C_{\text{nominal}} \times (f_{\text{linear}}/f_{\text{ferro}})^2$. The measurement chain was independently calibrated on a Tektronix MSO44B oscilloscope (1.5 GHz, 25 GSa/s; intrinsic rise time ≈330 ps after deconvolution). P-E hysteresis loops confirm the initial remanent polarization state ($BaTiO_3$ ≈0.25 C/m², coercive field ≈1.5 kV/cm) with no measurable degradation after repetitive operation, demonstrated up to 50 Hz at full performance and up to 200 Hz with an upgraded charging circuit. The resulting nanosecond pulses generate reduced electric fields (E/N) exceeding 500 Td, enabling efficient initiation of non-equilibrium plasma discharges, including fast streamer ignition and nanosecond repetitively pulsed (NRP) plasmas. Projected applications include HPM source excitation, EMC/EMP testing, and advanced nsPEF biomedical research. These results provide the first direct experimental evidence of inertial dynamical depolarization in bulk ferroelectrics and establish a practical platform for ultrafast plasma generation.

DOI: https://doi.org/10.31281/305nmp42

mihai.ganciu@ferrodynamics.com

I. INTRODUCTION

Pulsed-power technology underpins a broad class of applications-from directed-energy systems and high-power microwave (HPM) sources to non-equilibrium plasma reactors and biomedical devices-all of which demand fast-rising, high-amplitude voltage transients.

Building upon our recent demonstration of repetitive high-voltage generation via rapid thermal depolarization [1], here we present a qualitatively different approach based on electrically induced inertial dynamical depolarization described by the full Landau–Khalatnikov–Tani equation with polarization inertia [2–5].

Conventional architectures include Marx generators, spark-gap switches, and explosive ferroelectric generators (FEGs). Marx generators offer design flexibility but are typically constrained to rise times on the order of tens of nanoseconds. Explosive FEGs can deliver extraordinary peak energies yet are inherently single-use and introduce significant safety constraints [6,7]. Non-destructive ferroelectric generators based on thermal or mechanical depolarization overcome the single-use limitation, but their rise times seldom fall below several tens of nanoseconds and their repetition rates are restricted by thermal recovery [1,7].

A qualitatively different operating regime emerges from the LKT framework [2,5]: under fast high-voltage switching, a bulk ferroelectric capacitor can undergo a spontaneous inertial phase-space transition from a high-permittivity, overdamped state to a low-permittivity, high-Q underdamped state. Unlike classical ferroelectric switching, this bifurcation is governed by polarization inertia [3,4] and occurs on timescales far shorter than thermal relaxation.

The potential intersection with non-equilibrium plasma generation is particularly compelling. Atmospheric-pressure non-equilibrium plasmas-produced in dielectric barrier discharges (DBDs), pulsed corona reactors, and nanosecond repetitively pulsed (NRP) discharges-rely on brief, high-field excitation to create reactive species while maintaining a cool gas temperature [10–12]. The reduced electric field (E/N) achieved during the pulse rise determines the electron energy distribution and hence the selectivity of plasma-chemical reactions. Sub-5-ns rise times and high peak voltages, as demonstrated here, satisfy precisely the conditions required for efficient non-equilibrium ionization with minimal gas heating (“fast gas heating avoidance”) [14].

A central concern for any such claim is whether the observed fast transient genuinely reflects ferroelectric polarization dynamics or merely the passive RLC response of the charged capacitance discharging through the loop inductance and spark gap. We address this concern directly by means of two independent linear controls and a calibrated transmission-line reference source (Section IV). The measurement chain calibration and quantitative frequency-shift analysis provide the metrological foundation for attributing the dynamics to LKT inertial depolarization rather than circuit artifacts or other nonlinear dielectric effects (e.g., field-dependent permittivity or domain-wall motion alone).

In this revised manuscript we characterize the LKT dynamics, identify the separatrix as the governing control parameter, present experimental waveforms with quantitative metrics, and demonstrate through control experiments that the observed bifurcation and permittivity collapse are unique to the inertial ferroelectric response. We further discuss how these pulse characteristics translate into advantages for non-equilibrium plasma excitation [10–15], HPM generation [8,24], EMC/EMP testing [9], and biomedical nanosecond pulsed electric field (nsPEF) therapies [16–23].

To the best of our knowledge, this constitutes the first experimental observation of rapid inertial dynamical depolarization in bulk ferroelectric capacitors driven by fast electrical switching of a pre-charged capacitor, supported by independent linear controls and calibrated sub-nanosecond metrology.

II. PHYSICAL PRINCIPLE AND MODEL

The polarization dynamics of a ferroelectric element embedded in an RLC circuit are governed by the inertial Landau–Khalatnikov–Tani equation [2,5]:

$$M\ddot{P} + \gamma\dot{P} + \frac{\partial F}{\partial P} = E(t), \qquad (1)$$

where $F(P) = aP^2/2 + bP^4/4$ is the Landau free energy [3] with $a < 0$ below the Curie temperature T_C, M is the inertial coefficient of polarization [2,5], γ is the viscous damping coefficient, P is the polarization, and $E(t)$ is the applied field. In the classical (non-inertial) limit $M \equiv 0$, the dynamics are unconditionally overdamped [4]. Introducing a finite M opens an oscillatory degree of freedom characterized by a natural frequency ω_0 and quality factor $Q = M\omega_0/\gamma$.

At low applied fields the system resides in the overdamped regime ($Q < 1/2$): the effective permittivity is large, dissipation dominates, and polarization relaxes monotonically. Once the applied voltage exceeds a critical value V_C, the phase-space trajectory crosses a separatrix in $(P, \dot{P})$ space [1], triggering a spontaneous bifurcation into the underdamped regime ($Q \gg 1$). The effective permittivity drops sharply, the local oscillation frequency rises dramatically, and the circuit inductance together with the reduced residual capacitance form a high-frequency LC resonance. The abrupt release of stored polarization energy generates a steep voltage transient across the load.

The separatrix geometry-and hence V_C-depends on the Landau coefficients a and b, the inertial coefficient M, and the circuit parameters L and R [1,5]. This threshold can be empirically calibrated and electrically fine-tuned in real time, giving precise, shot-to-shot control of the bifurcation.

Physically, the double-well Landau potential [Fig. 1(a)] supports two stable polarization minima. The phase-space portrait [Fig. 1(b)] displays a separatrix separating overdamped relaxation from oscillatory dynamics. Crossing this boundary enables rapid depolarization and energy release, producing the nanosecond pulses illustrated in Fig. 1(c).

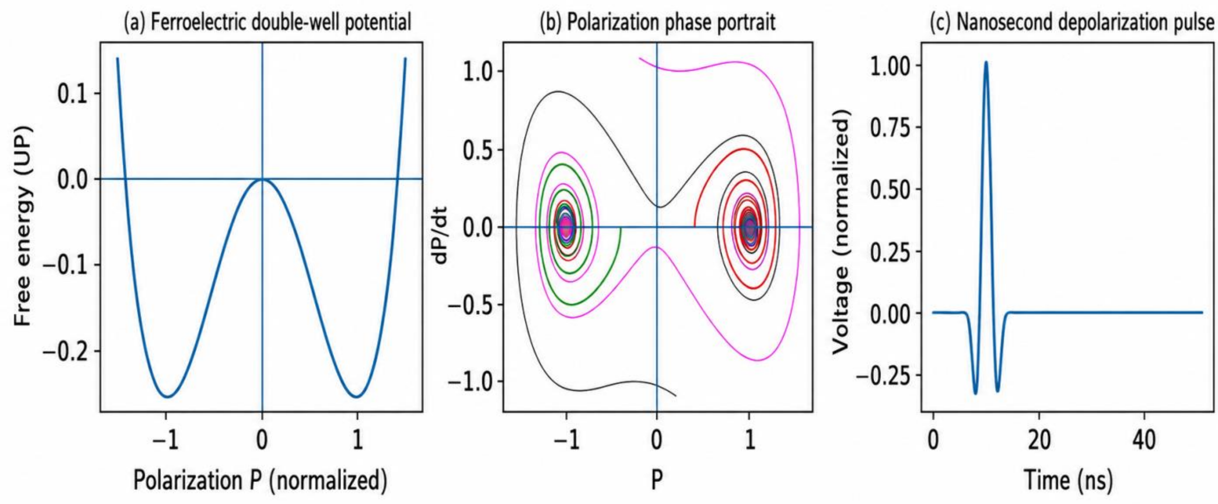

Figure 1: (a) Double-well Landau free energy describing ferroelectric polarization. (b) Phase-space trajectories predicted by the inertial LKT equation, showing the separatrix separating overdamped and oscillatory regimes. (c) Representative nanosecond voltage pulse produced by rapid depolarization of a ferroelectric capacitor.

III. SYSTEM ARCHITECTURE

The pulse generation system comprises five functional blocks: (1) a high-voltage charging circuit; (2) a protection diode and current-limiting resistor; (3) a bulk ferroelectric capacitor; (4) a low-parasitic RLC loop ($L \approx 30$–50 nH, $R \approx 0.3$–0.5 Ω); and (5) an ultra-fast spark gap coupling the circuit to the load. Polarization of the ferroelectric element is established by application of a DC field of 10 kV/cm. The stored voltage is then switched by opening the fast spark gap; the resulting spontaneous inertial transition is captured and routed to the load via a closed spark gap (triggered electrically or optically with a UVC-LED; switching time < 2 ns) [1]. Two load configurations were characterized. In Configuration A, the load is a non-inductive 50 Ω resistor inserted directly into the RLC loop, enabling clean waveform characterization of the overdamped-to-underdamped transition. Configuration B employs a 1:5 transmission-line pulse transformer (low primary inductance, secondary terminated into 50 Ω), yielding amplified output with high-frequency underdamped oscillations on the secondary-suitable for directly driving HPM sources such as vircators [8] or atmospheric plasma reactors [10].

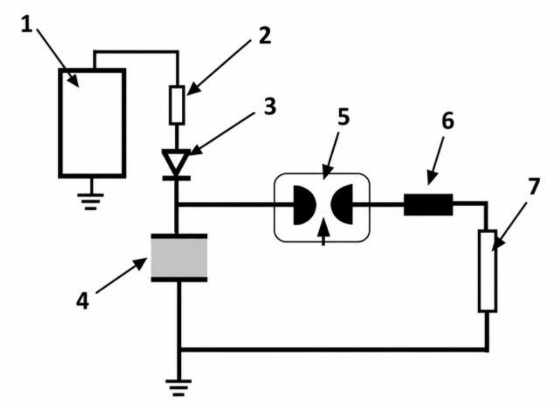

Figure 2: Schematic of the pulse generation system: (1) high-voltage charging circuit, (2) charging resistor, (3) protection diode, (4) ferroelectric capacitor, (5) ultra-fast spark gap, (6) equivalent inductance, and (7) load (resistive or 1:5 pulse transformer terminated into 50 Ω).

IV. CALIBRATED REFERENCE SOURCE AND INDEPENDENT CONTROLS

To establish metrological confidence in the fast-transient measurements and to discriminate true inertial ferroelectric dynamics from passive circuit ringing, we developed a transmission-line pulse generator that serves as an independent linear reference containing no ferroelectric element. The reference generator consists of a 50 Ω transmission line discharged through an ultrafast spark gap into a matched 50 Ω load, producing a clean monotonic pulse whose duration is set geometrically by the line length ($t = 2L/v$) and is therefore traceable to a length measurement.

The rise time of the reference pulse was measured on a Tektronix MSO44B oscilloscope (1.5 GHz bandwidth, 25 GSa/s) as 400–500 ps. After deconvolution of the instrument rise time (≈233 ps, using $t_{\text{meas}}^2 \approx t_{\text{signal}}^2 + t_{\text{scope}}^2$), the intrinsic signal rise time is approximately 330 ps. This independently confirms that the measurement chain faithfully resolves sub-nanosecond fronts well above the 90–200 MHz range of the ferroelectric transients.

Two independent linear controls support the inertial interpretation:

IV.a) Linear-dielectric control. The ferroelectric capacitor was replaced by a linear polypropylene-film capacitor of identical nominal capacitance (10 nF) in a physically identical circuit - same loop geometry, lead lengths, spark gap, and charging conditions. The polypropylene capacitor

produced a single damped oscillation at the fixed linear RLC frequency $f = 1/(2\pi\sqrt{LC})$, with amplitude scaling proportionally to charging voltage and **no threshold**. The ferroelectric capacitor, under identical conditions, oscillated at a markedly higher frequency - explainable only by a dynamic collapse of effective permittivity upon crossing the LKT separatrix, a behavior impossible for any linear dielectric.

IV.b) Spark-gap control. The transmission-line reference source employs an identical spark gap discharging into 50 Ω but contains no ferroelectric element. It produces a clean monotonic pulse with no underdamped high-frequency ringing, demonstrating that the spark-gap discharge alone does not generate the oscillatory dynamics observed with the ferroelectric capacitors.

Taken together, the simultaneous presence of (i) a reproducible voltage threshold V_C, (ii) a post-transition oscillation frequency higher than the linear RLC value - indicating dynamic permittivity collapse - and (iii) the absence of both features in two independent linear controls under otherwise identical conditions, constitutes experimental evidence that the observed dynamics are governed by inertial dynamical depolarization in the ferroelectric material and not by passive RLC resonance or other circuit nonlinearities.

V. EXPERIMENTAL RESULTS

Measurements were acquired with a Rohde & Schwarz RTE 1054 oscilloscope (500 MHz, 5 GSa/s) and, for the reference-source rise-time verification, with a Tektronix MSO44B oscilloscope (1.5 GHz bandwidth, 25 GSa/s). Ferroelectric materials studied include bulk $BaTiO_3$ and PZT (cylindrical, Ø50 × 20 mm). Initial polarization state and material integrity were verified by P-E hysteresis loop measurements before and after pulsed operation (remanent polarization consistent with literature values for $BaTiO_3$ ≈ 0.2–0.3 C/m²; no measurable degradation in coercive field or remanence after >10³ cycles at 50 Hz).

V.a) Ferroelectric transient (Configuration A)

At a charging voltage above V_C (typically 5 kV for the tested elements), the waveform across the 50 Ω series resistor shows a slow initial rise (overdamped phase) followed by an abrupt transition to high-frequency underdamped oscillations, in agreement with LKT predictions [1,5]. The 10–90% rise time of the leading edge is below 5 ns, and pulse amplitudes of 10–20 kV are routinely measured. At these parameters the peak reduced electric field delivered into a prospective plasma gap exceeds 500 Td, above the ionization threshold for atmospheric nitrogen [13].

V.b) Amplified transient (Configuration B)

With the 1:5 transmission-line transformer, the secondary displays underdamped oscillations with a sub-5-ns initial rise and amplitudes up to the 100–200 kV range. The oscillation frequency is consistent with the post-transition LC resonance predicted by the LKT model [1] for the measured effective capacitance and circuit inductance (≈30 nH). Operation is at room temperature, and no mechanical degradation of the ferroelectric element is observed after repeated cycles, confirming non-destructive behavior [3].

Figure 3: Reference pulse from the transmission-line generator, measured on a Tektronix MSO44B oscilloscope (1.5 GHz bandwidth, 25 GSa/s; date: 20 May 2026). Upper panel: rise-time histogram over 891 acquisitions, showing a distribution with minimum 472 ps, mean 1.022 ns, and standard deviation 379 ps. Lower panel: representative voltage waveform showing the fast leading edge (measured rise time 400–500 ps; ≈330 ps intrinsic after deconvolution). The low-amplitude oscillations visible after the leading edge reflect connection parasitics and are not characteristic of the generator output itself - they are of fixed frequency, threshold-free, and amplitude-proportional to the charging voltage, in sharp contrast to the high-frequency underdamped oscillations observed exclusively above V_C with the ferroelectric capacitors.

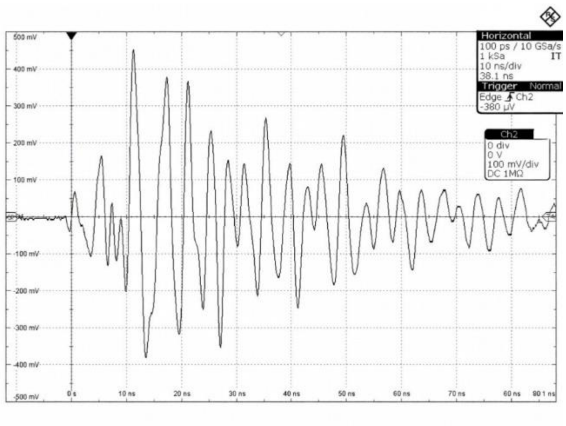

Figure 4: Experimental voltage waveform across the 50 Ω series resistor (Configuration A). The spontaneous overdamped-to-underdamped transition is visible; rise time < 5 ns. (Rohde & Schwarz RTE 1054, 500 MHz

We note that the two characteristic frequencies observed across configurations and materials (near 90 MHz and near 200 MHz) are consistent with different post-transition effective capacitances. Because $BaTiO_3$ and PZT differ in static permittivity and Landau coefficients, they are expected to settle to different low-permittivity states upon crossing the separatrix, and hence to different LC resonance frequencies for the same loop inductance. The frequency difference is therefore interpreted as a consequence of material-dependent permittivity collapse rather than as an inconsistency.

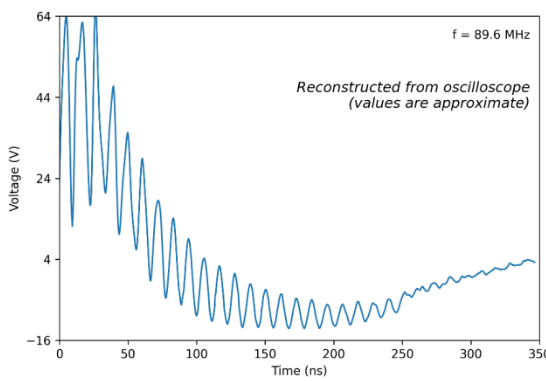

Figure 5: Voltage waveform on the 50 Ω secondary of the 1:5 pulse transformer (Configuration B), showing underdamped oscillations. (Rohde & Schwarz RTE 1054, 500 MHz.)

V.c) Threshold behavior

The critical threshold V_C manifests as a sharp, reproducible bifurcation: below V_C no fast transition occurs, while above V_C the transition is spontaneous and consistent across consecutive shots, validating the separatrix interpretation of the LKT model [1,5]. The existence of a voltage threshold is itself a nonlinear signature absent from any linear RLC circuit, in which amplitude scales proportionally with charging voltage and no qualitative transition occurs.

Material	Config.	V_{charge} (kV)	V_{pulse} (kV)	f_{osc} (MHz)	t_{rise} (10-90%)	Notes
$BaTiO_3$/PZT	A (50 Ω resistor)	5 (above V_C)	10–20	≈90	<5 ns	Threshold bifurcation; no transition in linear control
$BaTiO_3$/PZT	B (1:5 transformer)	20	100–200	≈200	<5 ns	High-Q underdamped; material-dependent post-transition C_{eff}
Linear PP control	Identical circuit	any	proportional	fixed RLC (lower)	-	No threshold, no frequency elevation
Transmission-line ref	-	-	monotonic	none	≈330 ps intrinsic	No ringing; metrology calibration standard

Table 1: Summary of key experimental parameters and controls. All ferroelectric data obtained at room temperature with repetitive operation up to 50 Hz (up to 200 Hz demonstrated with upgraded charging circuit); no degradation observed.

VI. DISCRIMINATING INERTIAL DEPOLARIZATION FROM LINEAR RLC RINGING

A natural objection is that the fast-rising transient followed by damped oscillations could arise from ordinary RLC ringing of the charged capacitance through the parasitic loop inductance and the spark gap, without invoking any polarization inertia. The two independent controls of Section IV directly refute this objection and also address potential contributions from field-dependent permittivity or domain-related nonlinearities in the ferroelectric.

VI.a) Linear-dielectric control

With the polypropylene capacitor the circuit exhibited the expected linear behavior: a single damped oscillation at a fixed frequency consistent with $f = 1/(2\pi\sqrt{LC})$, with amplitude scaling proportionally to the charging voltage and **no threshold**. With the pre-polarized ferroelectric capacitor of the same nominal capacitance, in the identical circuit, the post-transition oscillation occurred at a markedly higher frequency. Since L and the nominal capacitance are unchanged, the higher frequency can only be accounted for by a reduction of the effective capacitance during the underdamped regime - i.e., a collapse of the effective permittivity - precisely the behavior predicted by the inertial LKT model upon crossing the separatrix. A linear dielectric possesses no field-dependent permittivity that could collapse in this manner, nor does it exhibit a voltage threshold for bifurcation.

Quantitatively, the effective capacitance follows from the measured frequencies as

$$C_{\text{eff}} = C_{\text{nominal}} \times \left(\frac{f_{\text{linear}}}{f_{\text{ferro}}}\right)^2. \qquad (2)$$

VI.b) Spark-gap control

The transmission-line reference source of Section IV provides the second control. It employs an identical spark gap discharging into 50 Ω but contains no ferroelectric element, and produces a clean monotonic pulse with no underdamped high-frequency ringing. The oscillatory dynamics observed with the ferroelectric capacitors therefore cannot be attributed to spark-gap switching alone.

Taken together, the simultaneous presence of (i) a reproducible voltage threshold V_C, (ii) a higher post-transition oscillation frequency indicating dynamic permittivity collapse, and (iii) the absence of both features in two independent linear controls under otherwise identical conditions, constitutes experimental evidence that the observed dynamics are governed by inertial dynamical depolarization in the ferroelectric and not by passive RLC resonance of the external circuit or by generic nonlinear dielectric responses.

VII. DISCUSSION

The sub-5-ns rise times achieved here considerably exceed the performance of existing non-destructive ferroelectric generators (typically > 10–50 ns [7]) and are comparable to those of Marx generators of substantially greater complexity and footprint. The critical enabling ingredient is the inertial coefficient M in the LKT equation [2,5]: without polarization inertia, no bifurcation from overdamped to underdamped behavior can occur. This qualitatively distinguishes the present approach from prior ferroelectric generators based on thermal, mechanical, or classical-switching mechanisms [3,4,6,7].

VII.a) Non-Equilibrium Plasma Generation (Demonstrated Electrical Performance Enabling Projected Plasma Applications)

The demonstrated pulse characteristics - sub-5-ns rise time, peak voltages of tens to hundreds of kilovolts, and controllable oscillation frequency - are precisely the parameters that drive efficient non-equilibrium plasma formation. In nanosecond repetitively pulsed (NRP) discharges and dielectric barrier discharges (DBDs), the instantaneous reduced electric field E/N during the rise phase determines the mean electron energy and the branching ratio between ionization, dissociation, and vibrational excitation [10,11]. For atmospheric-pressure nitrogen/oxygen mixtures, peak E/N values above ~200 Td strongly favor ionization and the production of reactive oxygen and nitrogen species (RONS) [12,13].

The present system, with its rise time below 5 ns and tunable amplitude, can sustain peak E/N well above this threshold while keeping gas heating negligible - a regime sometimes described as "fast gas heating avoidance" in the NRP discharge literature [14]. Moreover, the underdamped oscillatory character of the post-transition waveform may be exploited to drive multi-pulse excitation within a single discharge event, potentially increasing plasma density without additional switching hardware. This is particularly attractive for surface dielectric barrier discharge (SDBD) actuators used in aerodynamic flow control [15], where compact, repetitive high-voltage sources are at a premium.

The repetition rate of up to 50 Hz has been demonstrated at full voltage and sub-5 ns rise time without degradation of the ferroelectric element. Using an upgraded charging circuit, repetitive operation up to 200 Hz has also been achieved. This confirms that the repetition rate is limited by the external charging electronics rather than by the ferroelectric material itself. Rates in the kilohertz range are projected with further optimization of the charging circuit. The demonstrated 50–200 Hz range is already sufficient for many plasma-chemical applications, including ozone synthesis, NOx reduction in flue gas, and plasma-assisted combustion [12]. We emphasize that **plasma generation itself is a projected application** based on the measured electrical parameters (E/N > 500 Td, sub-5 ns rise); direct plasma measurements (optical emission, discharge imaging, species densities) are the subject of ongoing work and are not claimed in this manuscript.

VII.b) HPM Generation (Projected)

The high-Q underdamped regime and sub-5-ns rise times are particularly advantageous for driving virtual-cathode oscillators (vircators) and other high-power microwave (HPM) sources. A rise time below 5 ns is critical for increasing vircator efficiency because it enables the rapid injection of beam current, allowing the virtual cathode to form almost instantaneously once the space-charge-limiting current is exceeded. This fast voltage ramp minimizes parasitic pre-breakdown processes and energy losses before virtual-cathode formation, and produces a more stable and coherent virtual cathode with higher beam modulation depth. Consequently, both the microwave conversion efficiency (beam-to-microwave) and the spectral purity of the radiated power are significantly improved, while shot-to-shot jitter is reduced [24].

Compared with conventional Marx-generator drivers (typical rise times 30–100 ns), the present generator offers a significantly faster leading edge while maintaining a compact footprint and repetitive operation up to 50 Hz. When coupled to a vircator designed for X-band (8–12 GHz) operation, the combination of sub-5-ns rise time, 100–200 kV amplitude, and controllable underdamped oscillations up to 200 MHz is projected to support peak radiated powers in the gigawatt range with improved shot-to-shot stability. The technology is equally relevant for other HPM configurations (MILOs, relativistic magnetrons) and for high-fidelity EMC/EMP testing compliant with MIL-STD-464 and MIL-STD-

188-125-1 standards. **No microwave radiation is measured in the present work**; the HPM relevance is stated as a projected application.

VII.c) Biomedical nsPEF Research (Projected)

Sub-5-ns pulses penetrate cell membranes with minimal Joule heating, enabling selective intracellular effects such as endoplasmic reticulum stress, organelle permeabilization, and immunogenic cell death [16,17]. Clinical and preclinical studies confirm nsPEF efficacy in irreversible electroporation of hepatocellular carcinoma [19], reduction of multi-drug resistance in pancreatic cancer [20], and treatment of lymphoma and colorectal cancer [21]. Sub-nanosecond regimes-now accessible with this source-are expected to further enhance intracellular targeting [17]. Additional demonstrated applications in related fields include stimulation of microalgae proliferation [23]. **Direct biomedical nsPEF experiments are projected**; the present work provides the enabling pulsed-power source.

VIII. CONCLUSION

We have demonstrated electrically induced inertial dynamical depolarization in ferroelectric capacitors as a practical mechanism for generating nanosecond, and potentially sub-nanosecond, high-voltage pulses at room temperature. The governing physics, encapsulated by the LKT equation with inertial coefficient M [2,5], account quantitatively for the observed spontaneous bifurcation from overdamped to high-Q underdamped behavior upon crossing the critical phase-space separatrix. Rise times below 5 ns, pulse amplitudes reaching tens to hundreds of kilovolts, and stable repetitive operation demonstrated up to 50 Hz at full performance, with capability extended to 200 Hz using an upgraded charging circuit, are achieved with $BaTiO_3$ and PZT capacitors without any destructive mechanism.

Independent linear controls (polypropylene capacitor and transmission-line reference) together with calibrated sub-nanosecond metrology establish that the dynamics originate from inertial polarization depolarization rather than passive circuit effects or generic nonlinear dielectric responses. The combination of sub-5-ns rise time, high peak voltage, and tunable oscillation frequency makes this source especially well-matched to non-equilibrium plasma excitation in NRP and DBD configurations, where high instantaneous E/N is required to maximize RONS production and minimize gas heating [10–15]. More broadly, these results establish a new, scalable paradigm for pulsed-power technology with applications spanning HPM generation [8,24], non-equilibrium plasma reactors [10–15], EMC/EMP testing [9], directed energy, and biomedical nsPEF therapies [16–23].

ACKNOWLEDGMENTS

The authors gratefully acknowledge PCT (Patent Cooperation Treaty) RO2026/050003 (M. Ganciu, A. Sebe, V. Cionga). The authors declare no conflicts of interest.

REFERENCES

[1] Ganciu, M., Cramariuc, O., Sebe, A. P., Mircioagă, R., & Ludu, A. (2026). Repetitive High-Voltage Pulse Generator Based on Thermally Depolarized Ferroelectrics. Romanian Cyber Security Journal, 8(1).

[2] Tani, H. (1959). Phenomenological Theory of Ferroelectrics. J. Phys. Soc. Jpn. 14, 777.

[3] Lines, M. E. & Glass, A. M. (1977). Principles and Applications of Ferroelectrics and Related Materials. Oxford University Press.

[4] Scott, J. F. (2000). Ferroelectric Memories. Springer.

[5] Richman, E. et al. (2017). Second-order Landau–Khalatnikov–Tani model for ferroelectric dynamics. J. Appl. Phys. 122, 094101.

[6] Shkuratov, S. I. et al. Explosive Ferroelectric Generator studies. DTIC Technical Reports (various years).

[7] Baird, J. et al. (2010). US Patent 7,560,855 B2; US Patent 7,999,945 B2.

[8] Benford, J., Swegle, J. A. & Schamiloglu, E. (2007). High Power Microwaves. Taylor & Francis.

[9] Giri, D. V. (2004). High-Power Electromagnetic Radiators. Harvard University Press / IEEE Press.

[10] Bruggeman, P. J. et al. (2016). Plasma–liquid interactions: a review and roadmap. Plasma Sources Sci. Technol. 25, 053002.

[11] Pai, D. Z. et al. (2010). Nanosecond repetitively pulsed discharges in air at atmospheric pressure: the glow regime. Plasma Sources Sci. Technol. 19, 065015.

[12] Fridman, A. (2008). Plasma Chemistry. Cambridge University Press.

[13] Adamovich, I. et al. (2017). The 2017 Plasma Roadmap: Low temperature plasma science and technology. J. Phys. D: Appl. Phys. 50, 323001.

[14] Rusterholtz, D. L. et al. (2013). Ultrafast heating and oxygen dissociation in atmospheric pressure nanosecond repetitively pulsed discharges. J. Phys. D: Appl. Phys. 46, 464010.

[15] Benard, N. & Moreau, E. (2014). Electrical and mechanical characteristics of surface AC dielectric barrier discharge plasma actuators applied to airflow control. Exp. Fluids 55, 1846.

[16] Nuccitelli, R. (2019). Application of Pulsed Electric Fields to Cancer Therapy. Bioelectricity 1, 30–36.

[17] Dong, Z. et al. (2025). Nanosecond Pulsed Electric Fields (nsPEFs) for Precision Intracellular Oncotherapy: Recent Advances and Emerging Directions. Int. J. Mol. Sci. 26(23), 11268.

[18] Chen, X. et al. (2025). Nanosecond Pulsed Field Ablation in Oncology: Advances and Efficacy. Medical Research Archives.

[19] Wang, Y. et al. (2025). Nanosecond pulsed electric field ablation as first-line curative therapy for hepatocellular carcinoma in high-risk locations. Int. J. Surg.

[20] Liu, Y. et al. (2023). Nanosecond pulsed electric field suppresses growth and reduces multi-drug resistance effect in pancreatic cancer. Sci. Rep.

[21] Guo, S. et al. (2019). Nanosecond Pulsed Electric Fields Induce Endoplasmic Reticulum Stress Accompanied by Immunogenic Cell Death in Murine Models of Lymphoma and Colorectal Cancer. Cancers 11, 1573.

[22] Reddy, V. et al. (2025). Pulsed electric fields: a sharp sword in the battle against cancers. Front. Immunol.

[23] Buchmann, L. et al. (2019). Effect of nanosecond pulsed electric field treatment on cell proliferation of microalgae. Bioresour. Technol. 271, 402–408.

[24] Li, L., Cheng, G. et al. (2011). Role of the rise rate of beam current in the microwave radiation of vircator. Journal of Applied Physics, 109(7), 074504. DOI: 10.1063/1.3560778.